Article

Offshore Wind and Wave Energy Complementarity in the Greek Seas Based on ERA5 Data

Kimon Kardakaris [1]**, Ifigeneia Boufidi** [1] **and Takvor Soukissian** [2,*]

1   School of Naval Architecture and Marine Engineering, National Technical University of Athens, Zografou Campus, 9, Iroon Polytechniou, 157 80 Zografou, Greece; kimonkardakaris@mail.ntua.gr (K.K.); ifigeneiaboufidi@mail.ntua.gr (I.B.)
2   Institute of Oceanography, Hellenic Centre for Marine Research, 190 13 Anavyssos, Greece
*   Correspondence: tsouki@hcmr.gr

Abstract: In this work, 20 years (2000–2019) of ERA5 wave and wind data are analyzed and evaluated for the Greek Seas by means of in-situ measurements derived from the POSEIDON marine monitoring system. Four different statistical measures were used at six locations, where in-situ wind and wave measurements are available from oceanographic buoys. Furthermore, the ERA5 wind and wave datasets were utilized for the estimation of the available wind and wave energy potential for the Greek Seas, as well as for the assessment of complementarity and synergy between the two resources. In this respect, an event-based approach was adopted. The spatial distribution of the available wind and wave energy potential resembles qualitatively and quantitatively the distributions derived from other reanalysis datasets. Locations with high synergy and complementarity indices were identified taking into account water depth. Finally, taking into consideration a particular offshore wind turbine power curve and the power matrix of the PELAMIS wave energy converter, the estimation of the combined energy potential on a mean annual basis is performed.

Keywords: offshore wind energy; wave energy; hybrid wind–wave energy; complementarity–synergy; Greek seas; ERA5

1. Introduction

Over recent decades, the global demand for energy has been rapidly increasing. This, in combination with the decline of fossil fuels, makes the need for renewable energy more urgent than ever. The marine environment is a vast source of renewable energy. Among the marine renewable energy (MRE) technologies, the most mature in terms of technological development and large-scale deployment is offshore wind energy [1]. On the other hand, onshore wind farms face strong social opposition and the most favorable siting locations have been occupied [2].

The main advantage the marine environment offers, regarding offshore wind turbines, is that the offshore winds are generally stronger and less variable, thus allowing operation at maximum capacity for a larger percentage of the time. However, the installation in deeper waters is an important factor, and mainly a current disadvantage, that determines to a great extent the high construction and maintenance costs [3,4]. Among the other forms of MRE, the exploitation of wave energy is also promising in areas with relatively calm wave climates, characterized thus by intermediate levels of power availability like the Mediterranean Sea [5]. In the relevant literature, it is usually considered that wave energy has some particular advantages such as small energy loss, better predictability, and higher energy density; see, for example [6–8].

1.1. Hybrid Offshore Wind–Wave Energy

A potential solution in order to compensate for the high installation and maintenance costs of offshore wind energy is through the development of hybrid systems that combine

offshore wind and an alternative marine renewable energy source (e.g., wave energy or offshore solar energy, etc.). Hybrid offshore wind–wave (WW) energy farms refer to wave energy extraction at the same marine space or on a shared platform with offshore wind turbines; see, e.g., [9,10]. See also the reviews in [11,12]. In this respect, there are several advantages as regards the development of hybrid WW energy farms that can provide important benefits such as:

(i)   The better utilization of the available marine space, whereas marine spatial planning, is an important prerequisite in this direction. For example [13] studied the joint exploitation of the WW resource for the Italian seas based on a marine spatial planning framework. A relevant assessment was performed for the island of Tenerife, where the optimal positions for collocating WW energy devices were examined taking into consideration the bathymetry and the distance from ports [14]. In [15], a review on the multiple-use of marine space is presented.

(ii)   The reduced power variability, especially for locations where wind and wave resources are not strongly correlated. These aspects were recently investigated in a multisite analysis in [16], using field observations of met-ocean conditions. It was found that the reduction in variability depends on the magnitude and lag of resource correlation and the wind–wave capacity mix of the particular location, rendering thus hybrid systems more beneficial in certain locations than others; see also [17,18]. Furthermore, Ref. [19] studied the WW resource for the Black Sea, Ref. [20] for specific locations at the coasts of Ireland, and [21] for the European seas.

(iii) The enlargement of weather windows for operation and maintenance [11,22]. Moreover, wave energy converters (WECs), acting as wave barriers, can create a wave shadow area where wind turbines can be installed in milder sea state conditions [22].

(iv)   The decrease in the potential environmental impacts compared to the impacts of the stand-alone installations [23].

Collocation of WECs with offshore wind turbines is also advantageous in financial terms (e.g., by using the same grid infrastructure and port facilities, following a common consenting process, increasing the capacity factor of the installation, etc.). See also the relevant discussion in [11,24].

In order to identify suitable offshore areas for a hybrid WW installation, it is necessary to evaluate the impact of the combined use on the variability of the final total energy output. This is usually quantified through exploitability indices, which combine information on the availability of wind and wave energy, along with the degree of correlation between the two resources [25]. The assessment of co-located WW farms off the Danish coast was studied in [18]. An approach based on the assessment of the available resources and technical constraints was developed by implementing the Co-Location Feasibility (CLF) index that takes into account not only the available power, but also the correlation between the resources and the power variability.

Sustainability indices have also been investigated for the co-location of offshore wind farms and aquaculture plans [26], whereas wave energy, offshore wind energy and aquaculture activities were studied in the Canary Archipelago, resulting in a methodology and a useful tool to mapping the co-location opportunities [27]. In order to examine a combined WW energy farm, Ref. [17] examined real meteorological data to determine the difference in power performance between a wind turbine combined with a number of WECs than a single wind turbine. They concluded that the power variability (i) is reduced in the case of the combined resources for any number of WECs and (ii) the two resources exhibit really good complementarity that is, however, strongly dependent on the site selection.

1.2. Synergy and Complementarity

In the feasibility studies for hybrid WW energy farm development, complementarity is one of the most important aspects.

Regarding complementarity and synergy assessment between renewables in general, there are several studies in the relevant literature, examining in particular wind and solar power onshore or offshore. Such studies were conducted in Italy using high-resolution data, while apart from the assessment of spatial and temporal complementarity, its scale is approached via Monte Carlo simulation [28]. In [29], the possibility of the combined use of solar and wind energy over Europe is assessed, examining also the complementarity at different time scales using 3-year long time series. In [30], a study for the complementarity of wind and solar resources over Mexico is performed using GIS-based software with high-resolution maps. A systematic quantitative analysis of the complementarity characteristics of solar and wind resources on the Australian continent is performed in [31], exhibiting the spatio-temporal synergy of the two sources, while in [32], the spatio-temporal complementarity of solar and wind power is studied at different time scales for Germany. Relevant assessments were also carried out for offshore regions of China, where wind power is always negatively correlated with photovoltaic power on the hourly, daily and monthly time scales [33]. Recently [24] assessed in-depth offshore wind and solar complementarity aspects for the Mediterranean basin using ERA 5 reanalysis data. A review as regards complementarity/synergy between renewable energy sources is provided in [34].

However, for the assessment of the synergistic characteristics of WW power, there is very limited related work, as opposed to the ones about wind and solar, especially over the marine environment of the Greek seas [35]. Specifically, an investigation of the combined use of WW power for remote islands in Greece, was conducted in [36], using stochastic processes, without, however, a further assessment on their complementarity. The site selection for hybrid offshore WW energy systems in the Greek seas was studied in [37] based on the Analytic Hierarchy Process (AHP) method where environmental impacts have also been assessed.

The structure of this paper is the following: In Section 2, the ERA5 reanalysis wind and wave data for the Greek Seas that was used in the analysis are described and evaluated against in-situ measured data obtained from oceanographic buoys. In Section 3, the theoretical background of an event-based complementarity and synergy analysis is presented in brief. In Section 4, the numerical results of this work are presented and discussed. As a first step, the offshore wind and wave power potential is estimated and then, the complementarity and synergy indices are calculated for the examined area, while the water depth was also taken into consideration. In addition, a realistic application is presented, considering an actual wind turbine and an attenuator WEC at the most favorable locations regarding synergy/complementarity. Finally, in Section 5 some concluding remarks are provided.

2. ERA 5 Reanalysis Data and Initial Evaluation

In this section, the ERA5 reanalysis wind and wave dataset is described and evaluated for the Greek Seas, by using in-situ measured data obtained from six oceanographic buoys.

2.1. ERA5 Dataset

Produced by the European Centre for Medium-Range Weather Forecasts (ECMWF), the ERA5 reanalysis dataset combines vast amounts of historical observations into global estimates using advanced modeling and data assimilation systems [38]. Moreover, it provides hourly estimates of a large number of atmospheric, land and oceanic climate variables, covering the Earth on a ~30 km grid and resolving the atmosphere using 137 levels from the surface up to a height of 80 km. The data can be freely accessed from the Copernicus Climate Data Store (https://cds.climate.copernicus.eu/, (accessed on 3 March 2021) see also https://www.ecmwf.int/en/forecasts/datasets/reanalysis-datasets/era5, (accessed on 3 March 2021) [38,39].

Regarding ERA5 wind and wave data, in [40] sea surface wind speed data over the Caspian Sea were evaluated in comparison with measurements from offshore platforms and showed good agreement for measurements greater than 2 m/s. In [41] wind speed data over the South and Southeast Brazilian coastline from ERA5 and two more reanalysis

datasets were compared against in-situ measurements and concluded that ERA5 has a better performance. Furthermore, in [42], ERA5 wave data were compared to an observed wave dataset collected offshore in the swell-dominated region of the Oman coast in the western Arabian Sea. It was concluded that a finer grid than the one provided by the ERA5 wave dataset is necessary to fully model the complexity of the region.

In this work, 20 years (1 January 2000–31 December 2019) of available wind and wave data were utilized for the Greek Seas (defined by a rectangle with the top left corner at 42° N, 19° E and bottom right corner at 33° N, 30° E). For the significant wave height and the wave energy period the data are provided on a 0.50 × 0.50° spatial grid, while for the wind speed, the data are available at 100 m height (i.e., at a typical wind turbine hub height) on a 0.25° × 0.25° spatial grid; see [39].

2.2. In-Situ Measurements

In-situ measurements are provided by the POSEIDON marine monitoring network in the Greek seas. POSEIDON system was established in 1999 and comprises of oceanographic buoys, deployed in deep water locations, https://poseidon.hcmr.gr/ (accessed on 7 June 2021); see also [43,44]. The buoys measure the most important spectral wave parameters (significant wave height, spectral peak period and mean wave direction) as well as wind speed and direction at a height of 3 m above the sea surface. Buoy measurements were widely considered as the primary reference data source for model-generated and satellite wind validation; see, e.g., [45–48]. It is worth mentioning that buoys measure temporal averages at a specific location while model-generated data refer to instantaneous spatial averages. An important disadvantage of the measurements obtained from buoys is their limited spatial coverage, a drawback which is partly compensated by the increased measurement accuracy [49].

For the evaluation of ERA5 data, in-situ wind and wave measurements are obtained and analyzed from six buoys deployed in the following locations: Mykonos [37.51° N, 25.46° E], Lesvos [39.15° N, 25.81° E], Santorini [36.26° N, 25.50° E], Athos [39.96° N, 24.72° E], Pylos [36.83° N, 21.62° E], and Zakynthos [37.95° N, 20.60° E]; see Figure 1 and Table 1. Wind measurements are averaged over a recording period of 600 s with a sampling frequency of 1 Hz and a recording interval of 3 h. Wave measurements have a recording period of 1024 s, sampling frequency 1 Hz and recording interval 3 h. Buoy records exhibit gaps of various lengths due to software malfunctioning, hardware damage, etc.; nevertheless, the number of available records is sufficient to carry out the statistical analysis.
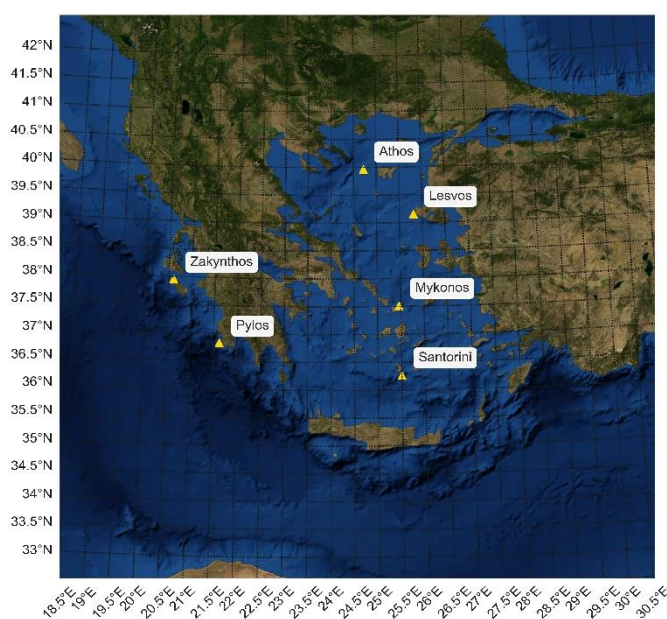

Figure 1. Location of the POSEIDON buoys.

Table 1. POSEIDON buoy locations and measurement period.

Buoy Location	Coordinates	Measurement Period
Mykonos	37.51° N, 25.46° E	1999–2012
Lesvos	39.15° N, 25.81° E	1999–2012
Santorini	36.26° N, 25.50° E	1999–2012
Athos	39.96° N, 24.72° E	2000–2015
Pylos	36.83° N, 21.62° E	2007–2015
Zakynthos	37.95° N, 20.61° E	2008–2011

2.3. Data Reparation

In order to compare wind and wave data from both sources, the corresponding time series have to be co-located in the spatial and temporal domain. Therefore, all the data were fixed to the 3-h resolution (corresponding to the recording interval of the in-situ data). Subsequently, the ERA5 reanalysis dataset was spatially co-located with the buoy data via the nearby grid point values by using a simple form of inverse squared distance weighting interpolation function based on the values of the four nearest grid points; see, e.g., [49]. Denoting x_1, x_2, x_3 and x_4 the respective variables (wind or wave parameters) at the four grid points surrounding the buoy location, and r_1, r_2, r_3 and r_4 the corresponding distances from that location, the requested data for each variable at the specific buoy location can be estimated as follows:

$$x = \frac{\sum_{i=1}^{4} \frac{x_i}{r_i^2}}{\sum_{i=1}^{4} \frac{1}{r_i^2}} \qquad (1)$$

It is worth mentioning that for the buoy in Pylos, the estimation of the examined wave parameters took into consideration only three grid points, as one of the four nearby locations was onshore and thus it was impossible to include it in the calculation procedures.

For wind speed comparison and evaluation purposes, the common reference height above the sea surface was set at 3 m for both wind data sources. To enable the comparison, the ERA5 wind speed data were adjusted to 3 m height from the surface by using the following equation:

$$u_{h_2} = u_{h_1} \frac{\ln\left(\frac{h_2}{z_0}\right)}{\ln\left(\frac{h_1}{z_0}\right)} \qquad (2)$$

where u_{h_2} (m/s) is the calculated wind speed at height h_2 (m), u_{h_1} (m/s) is the known wind speed at height h_1 (m), and z_0 (m) is the roughness length equal to 0.0002 m for neutral atmospheric conditions.

Regarding wave data, the in-situ wave period measurements refer to the spectral peak period T_p. Under the JONSWAP spectrum with a peak enhancement $\gamma = 3.3$, T_p and the wave energy period T_e are approximately related as follows:

$$\frac{T_e}{T_p} \approx 0.9 \qquad (3)$$

see also [50].

2.4. Data Evaluation

In order to evaluate the performance of the ERA5 reanalysis dataset, four different statistical measures were adopted for every variable and measuring station, e.g., Root Mean Squared Error (*RMSE*), Mean Bias Error (*MBE*), or simply bias, Pearson correlation

coefficient (r), and Mean Absolute Error (*MAE*). *RMSE*, *MBE* and *MAE* are, respectively, defined as follows:

$$RMSE = \sqrt{\frac{1}{n} \sum_{i=1}^{n} \left(X_i - \hat{X}_i\right)^2} \tag{4}$$

$$MBE = bias = \frac{1}{n} \sum_{i=1}^{n} \left(X_i - \hat{X}_i\right) \tag{5}$$

$$MAE = \frac{1}{n} \sum_{i=1}^{n} \left|X_i - \hat{X}_i\right| \tag{6}$$

where X_i denotes the measured parameter obtained from the buoy and $\hat{X}_i$ the corresponding parameter obtained from the ERA5 dataset. *RMSE* is actually the standard deviation of the errors (also referred to as prediction errors), between the "true" values of a variable (i.e., the $X_i's$) and the corresponding values obtained from experiments (i.e., the $\hat{X}_i's$). In this respect, *RMSE* provides a measure of the spread of $X_i - \hat{X}_i$. *MBE* (bias) is the mean error between the $X_i's$ and $\hat{X}_i's$, and *MAE* is the corresponding mean absolute error (absolute bias). The above-mentioned measures provide different forms of absolute error between the two data sources.

For the estimation of the corresponding relative errors, the relative error *RE* and the scatter index *SI* are also introduced:

$$RE = \frac{100}{n} \sum_{i=1}^{n} \frac{\left(X_i - \hat{X}_i\right)}{X_i} \tag{7}$$

$$SI = \frac{\sqrt{\frac{1}{n} \sum_{i=1}^{n} \left(X_i - \hat{X}_i - MBE\right)^2}}{\overline{X}} \tag{8}$$

respectively, where $\overline{X}$ denotes the mean value of X.

The lower the values of the metrics provided in Equations (4)–(8), the better the agreement between X and $\hat{X}$.

As an indicative result, in Figures 2–4, the scatter diagrams of H_S, T_e and u_W at 100 m asl, as obtained from buoys and ERA5 dataset along with the corresponding regression lines for two locations in the northern Aegean Sea (Athos) and Ionian Sea (Pylos) are, respectively, provided. The estimation of the regression lines was performed using the ordinary least squares method, after excluding outliers. The identification of the outliers was based on the Cook's distance criterion, i.e.,

$$CD_i = \frac{\sum_{j=1}^{n} \left(\hat{y}_j - \hat{y}_{j(i)}\right)^2}{s^2}, \ i = 1, 2, \cdots, n, \tag{9}$$

where n is the number of data points, $\hat{y}_{j(i)}$ is the fitted response value (i.e., the values of ERA5 dataset) obtained after excluding the i-th observation, and s^2 is the mean squared error.

The corresponding statistical results for H_S, T_e and u_W are summarized in Tables 2–4, respectively.

The ERA5 reanalysis dataset, in general, tends to underestimate the actual values of the examined parameters. Specifically, *MBE* is positive in all locations (except for Santorini) and for all wind and wave parameters examined (except for u_W in Athos). Furthermore, the correlation coefficient values take values well above 0.8 for every case (except for Santorini as regards T_e and Pylos, Zakynthos as regards u_W), which indicates a rather strong correlation between the two data sources.

The largest relative errors regarding wave parameters are encountered in Pylos (26.26% for H_S and 23.6% for T_e), while the scatter index *SI* takes its maximum values (0.308 for H_S and 0.183 for T_e) at Santorini. For wind speed, the largest relative error, in absolute terms, corresponds to Athos (−34.69%) and the largest scatter index (0.406) to Zakynthos.
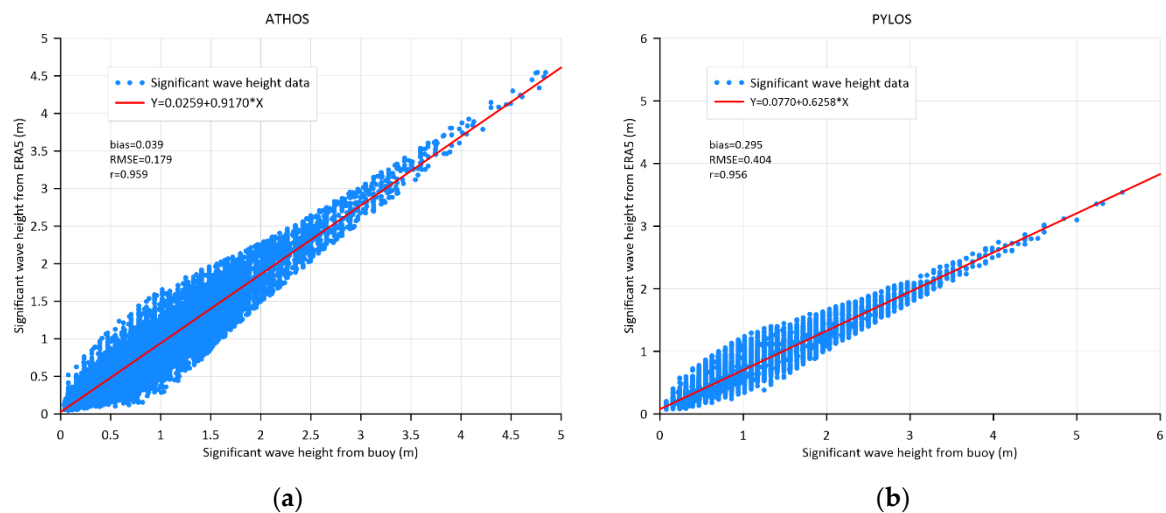
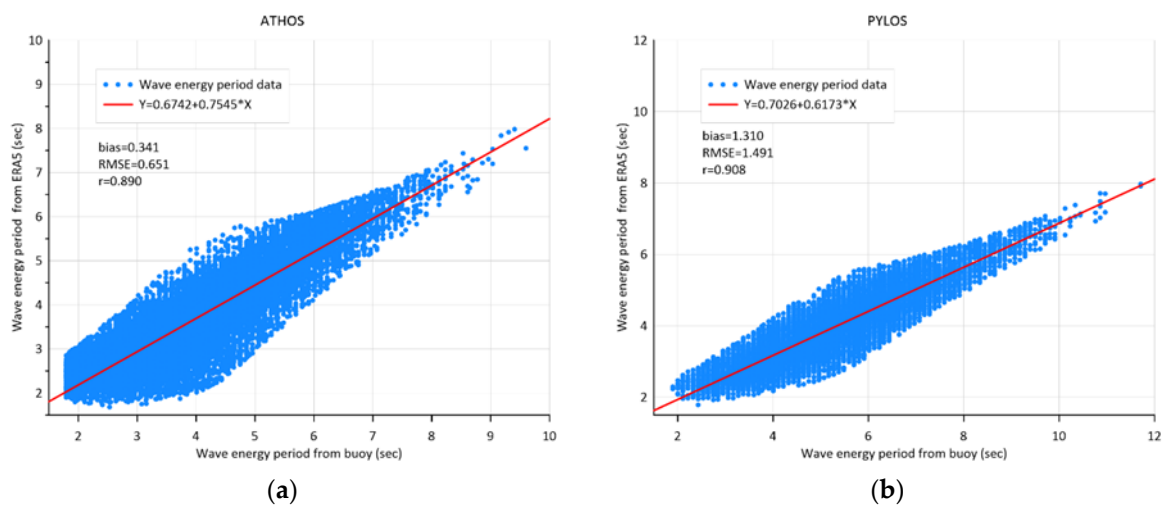**Figure 2.** Scatter plots of H_S obtained from buoy and ERA5 dataset for Athos (**a**) and Pylos (**b**).

Figure 3. Scatter plots of T_e obtained from buoy and ERA5 dataset for Athos (**a**) and Pylos (**b**).
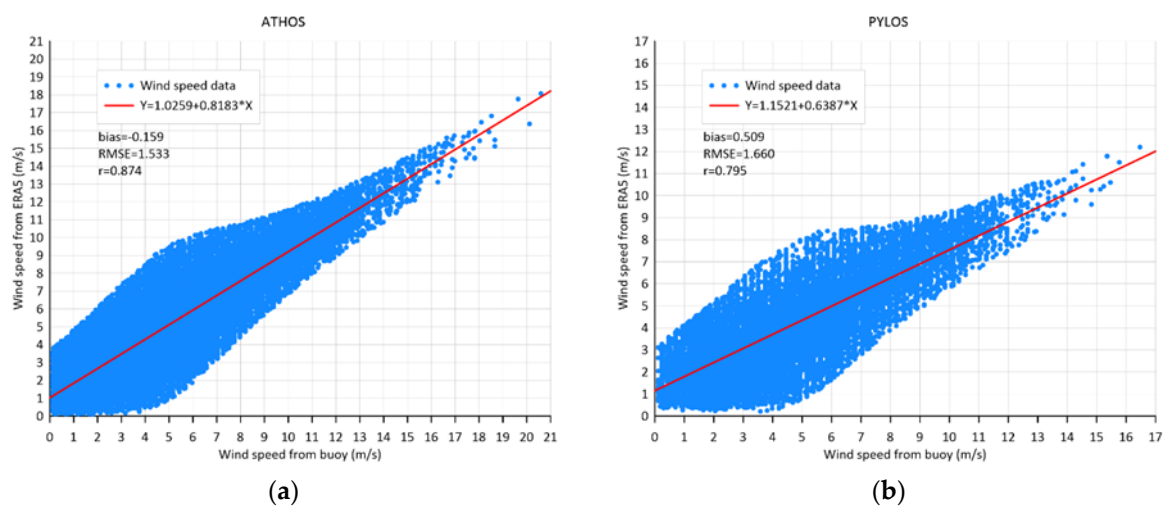

Figure 4. Scatter plots of u_W obtained from buoy and ERA5 dataset for Athos (**a**) and Pylos (**b**).

Table 2. Results of data evaluation of the significant wave height H_S obtained from ERA5 and in-situ measurements.

Parameter	Athos	Mykonos	Pylos	Santorini	Lesvos	Zakynthos
RMSE	0.179	0.272	0.404	0.306	0.201	0.186
MBE	0.039	0.025	0.295	−0.157	0.030	0.024
r	0.959	0.922	0.956	0.873	0.905	0.935
MAE	0.132	0.205	0.307	0.232	0.148	0.142
RE (%)	−1.304	−11.969	26.263	−23.392	2.868	2.692
SI	0.224	0.274	0.278	0.308	0.276	0.234

Table 3. Results of data evaluation of the wave energy period T_e obtained from ERA5 and in-situ measurements.

Parameter	Athos	Mykonos	Pylos	Santorini	Lesvos	Zakynthos
RMSE	0.651	0.808	1.491	0.822	0.638	0.898
MBE	0.341	0.200	1.310	−0.131	0.294	0.478
r	0.890	0.832	0.908	0.731	0.870	0.877
MAE	0.522	0.641	1.318	0.672	0.508	0.743
RE (%)	6.328	−0.741	23.628	−7.238	4.826	6.553
SI	0.134	0.176	0.136	0.183	0.139	0.158

Table 4. Results of data evaluation of the wind speed u_W obtained from ERA5 and in-situ measurements.

Parameter	Athos	Mykonos	Pylos	Santorini	Lesvos	Zakynthos
RMSE	1.533	1.627	1.660	1.641	2.025	1.959
MBE	−0.159	0.232	0.509	−0.249	0.829	0.309
r	0.874	0.879	0.795	0.821	0.807	0.716
MAE	1.220	1.326	1.350	1.309	1.649	1.566
RE (%)	−34.687	−19.405	−9.060	−25.459	−6.471	−25.932
SI	0.320	0.235	0.344	0.287	0.305	0.406

It should be noted here that a part of the discrepancies derived from the above analysis, might be attributed to the following reasons: (i) the measured energy wave period T_e, is not a direct result from wave spectral analysis, but is obtained by the approximate relation (3); (ii) the wind speed u_W at 100 m asl, is a result obtained from the measured wind speed at 3 m asl by using the approximate relation (2). On the other hand, it can be seen that the performance of ERA5 is strongly site-dependent. As a general conclusion, it can be stated that the ERA5 dataset underestimates the wind and wave conditions in the Greek Seas. However, for the scope of this work, the ERA5 dataset performs satisfactorily compared to buoy measurements, since the deviations are almost all acceptable; the detailed evaluation of ERA5 wind and wave datasets is an undergoing activity of the authors.

3. Wind and Wave Synergy and Complementarity

Let us first define the most important wind and wave power characteristics. The wind power incident on a surface A is provided by the following equation:

$$WP = \frac{1}{2}\rho A u_W^3 \tag{10}$$

where ρ is the atmospheric density that is considered constant and equal to 1.225 kg/m^3, A is the vertical to the wind speed surface for which the power is calculated, and u_W is the wind speed in m/s. For $A = 1$ m^2, the wind power density is obtained; this quantity will be used in the rest analysis and will be simply denoted as WP.

The wave energy flux per unit length of wave front (also known as wave power density or wave energy potential) is defined as follows:

$$VP = \frac{\rho g}{64\pi} H_S^2 T_e \cong 0.49 H_S^2 T_e \text{ (in kW/m),} \tag{11}$$

where ρ is the density of seawater that is considered constant and equal to 1025 kg/m^3, g is the gravitational acceleration equal to 9.8066 m/s^2, H_S is the significant wave height in m, and T_e is the wave energy period in s.

For the complementarity/synergy analysis, we will follow the event-based approach that was presented in [24]; see also [31].

Specifically, some lower thresholds regarding the mean annual offshore wind and wave power potential, WP_L and VP_L, respectively, should be introduced. In principle, the locations that are of interest are the ones that satisfy the following conditions: $WP_{AN} > WP_L$ and $VP_{AN} > VP_L$, where WP_{AN} and VP_{AN} denote the mean annual wind and wave power density, respectively.

Then, the wind to wave complementarity index WCV, is defined as follows:

$$WCV = \Pr\left[[WP_{AN} > WP_L] \cap [VP_{AN} \leq VP_L]\right] \tag{12}$$

In this case, it is clear that if the mean annual wave power density is below the corresponding lower threshold VP_L, but the mean annual wind power density is above the corresponding lower threshold WP_L, then energy from wind complements energy from wave. For the estimation of this index, the mean annual wind and wave densities (for all examined years) should be estimated and compared to the corresponding lower thresholds. Then WCV can be estimated as the frequency of occurrence of the compound event $[WP_{AN} > WP_L] \cap [VP_{AN} \leq VP_L]$. In a similar way, the wave to wind power complementarity index VCW, can be defined as follows:

$$VCW = Pr\left[[WP_{AN} \leq WP_L] \cap [VP_{AN} > VP_L]\right] \tag{13}$$

Large values of the above indices suggest that the corresponding resources are strongly complementary, while low values denote poor complementarity.

Moreover, the following events can be also defined:

$$E_W = [WP > WP_L], \; E_V = [VP > VP_L] \tag{14}$$

Using the above events E_W and E_V, and the exclusive OR operator, the synergy index of wind and wave power, SWV is defined as follows:

$$SWV = Pr[E_W \oplus E_V] \tag{15}$$

where $\oplus$ denotes the exclusive OR operator. This operator yields true if exactly one of E_W, E_V is true. The operator yields false if both E_W, E_V are true or both are false. For the estimation of the synergy index, the instantaneous events WP and VP should be firstly compared with respect to the corresponding lower thresholds WP_L, VP_L. Then SWV can be estimated as the frequency of occurrence of the compound event $[WP > WP_L] \oplus [VP > VP_L]$ for the examined time series. Values of SWV close to 1 suggest areas that are highly synergetic, while low synergetic areas are characterized by values of SWV close to zero.

Moreover, the joint non-availability of wind and wave power index UWV, is defined as follows:

$$UWV = Pr\left[[WP_{AN} \leq WP_L] \cap [VP_{AN} \leq VP_L]\right] \tag{16}$$

where a value of UWV close to 1 indicates that the specific area is out of consideration regarding the joint development of offshore wind and wave energy.

The adopted lower thresholds WP_L and VP_L, are 280 W/m^2 and 5 kW/m, respectively.

4. Results

4.1. Offshore Wind and Wave Power Potential

In order to identify potentially more promising grid points for the co-exploitation of WW energy, it is necessary to assess first the two sources separately.

The spatial distributions of the mean annual wind and wave power potential of the Greek seas based on the ERA 5 datasets are presented in Figure 5a,b, respectively.
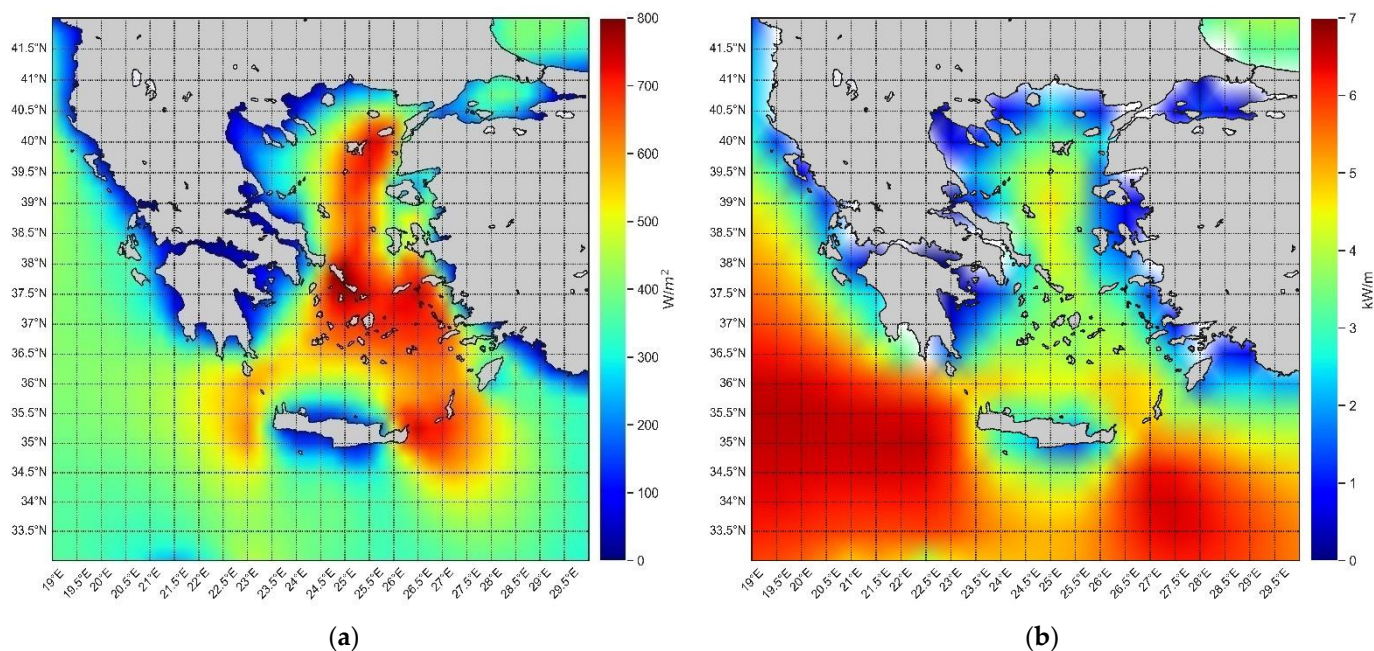

Figure 5. Offshore wind (**a**) and wave energy (**b**) potential.

From Figure 5a it is evident that the highest wind power density values (650–800 W/m^2), are encountered across the central axis of Aegean Sea, namely from Limnos and Samothraki Isl. up to the Cyclades complex, and from Samos and Ikaria Isl. up to the straits between Crete and Kasos Isl. These areas are characterized by strong winds during winter and the Etesian winds (seasonal winds of northern direction) during summer. Wind power potential values ranging between 500–600 W/m^2 are observed mainly in the straits of Crete and Kythira Isl. These results are in fair agreement with those provided in [51], where an Eta-based numerical atmospheric model of the POSEIDON system with a higher resolution (0.1 deg $\times$ 0.1 deg) was used.

Wave energy flux (see Figure 5b), ranges between 5–7 kW/m in west, southwest and southeast areas of Crete Isl. (areas between Crete and Kithira Isl., and Karpathos and Kasos Isl., respectively). These areas are characterized by large fetch lengths that lead to larger wind waves and swells. Although the Aegean Sea is an area characterized by strong winds, the presence of many islands limits the wind fetch blocking swells from being developed. Consequently, wave energy flux values are relatively low (3–5 kW/m). These results are quantitatively and qualitatively in fair agreement with the results of [52], who studied ten years of data obtained from the WAM-Cycle 4 numerical wave simulation model with a higher resolution (0.1 deg $\times$ 0.1 deg).

4.2. Synergy and Complementarity between Offshore Wind and Wave Energy

In this section, the assessment of the most favorable locations in terms of complementarity and synergy is examined. Specifically, in Figure 6, the complementarity indices *WCV* and *VCW* are provided, along with the synergy index *SWV* and the joint non-availability of wind and wave power index *UWV*. The areas characterized by strong wind to wave complementarity (i.e., high values of *WCV*) are encountered across the central and eastern

Aegean Sea, as well as in straits between Crete and Rhodes Isl. and between Crete Isl. and Peloponnesus. The overall maximum value of *WCV* is 45.143% and corresponds to the location (38.00° N, 26.50° E), at a water depth of ~325 m. The areas characterized by strong wave to wind complementarity (i.e., high values of *VCW*) are located very offshore in the southern Ionian Sea. The overall maximum value of *VCW* is 9.987% and corresponds to the location (33.00° N, 21.50° E), at a water depth of ~1008 m. Relatively high values of synergy between wind and wave are encountered across the central Aegean Sea, the western and eastern offshore areas of Crete Isl. and in offshore areas of the Ionian Sea. The overall maximum value of *SWV* is 31.072% and corresponds to the location (35.00° N, 27.00° E), at a water depth of ~3151 m. Finally, the joint non-availability of wind and wave power index takes very high values across almost all coastal areas of Greece.
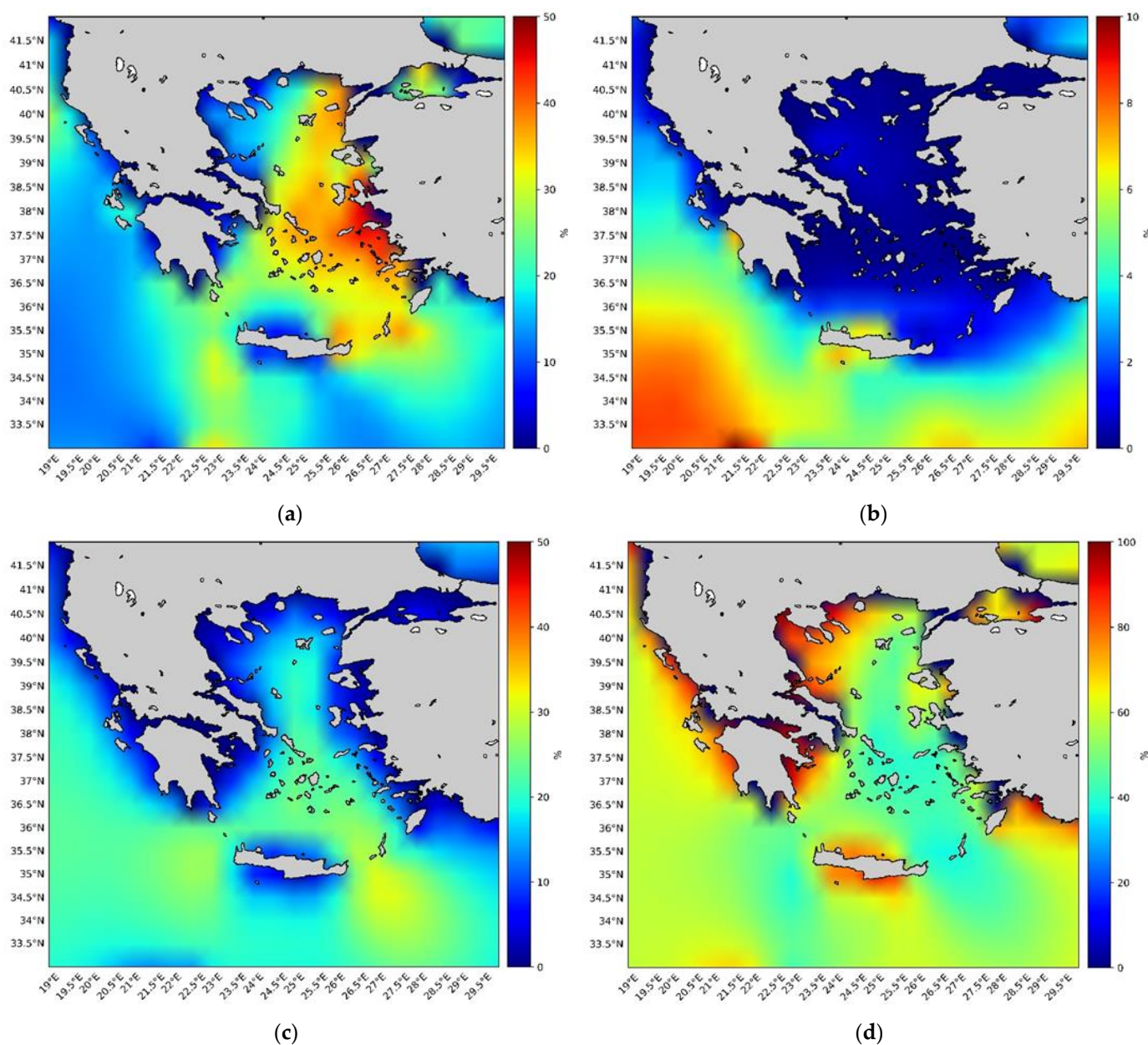

Figure 6. Spatial distribution of *WCV* (**a**), *VCW* (**b**), *SWV* (**c**) and *UWV* (**d**).

Based on the theory presented in Section 3 and the results depicted in Figure 6, 50 locations characterized by the highest values of wind to wave complementarity (Figure 6 a) and synergy (Figure 6c) indices were identified. From these locations, the ones with water

depths greater than 300 m were excluded from further analysis. This is in agreement with [53], where it is stated that "*The considered water depth is between 200 and 300 m, which is the deep-water range used in the current floating offshore wind turbine (FOWT) industry*". Let it be noted however that, regarding the offshore oil and gas sector, the relevant water depths refer to the level of thousands of meters [53].

The bathymetry data of the examined region were derived from the European Marine Observation and Data Network (EMODnet—https://portal.emodnet-bathymetry.eu/ (accessed on 21 July 2021)). Moreover, locations very close to the shore were also excluded from further analysis.

In Figure 7a, the grid points (of depths less than 300 m), exhibiting the highest values of complementarity index *WCV* between offshore wind and wave energy are shown. There are 23 locations with depths less than 300 m exhibiting the highest values of wind to wave complementarity. Note that all points are located in the Aegean Sea, while the location with the overall highest value of complementarity index (45.143%) is located southeast of Chios Isl. (38° N, 26.5° E). In Figure 7b eight grid points (of depths less than 300 m) that exhibit the highest values of synergy index *SWV* are depicted. All points are located in the southern Aegean Sea, except from point (35° N, 27.5° E) that exhibits the highest value of synergy index (29.261%) and is located southeast of Karpathos Isl.
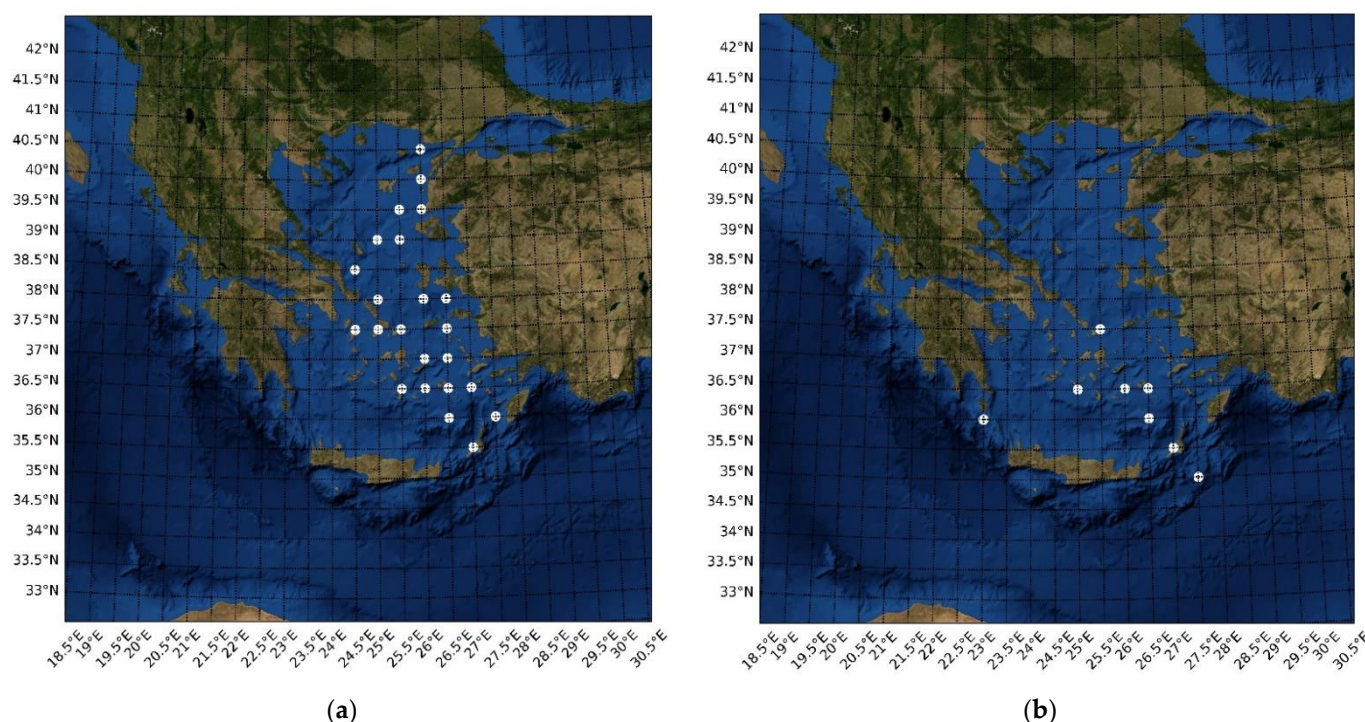

(**a**)　　　　　　　　　　　　　　　　(**b**)

Figure 7. Locations with the highest values of wind to wave complementarity (**a**) and synergy (**b**) indices.

4.3. An Actual Application

For the exploitation of offshore wind energy, the Vestas V164-8.0 (an 8-MW offshore wind turbine specifically designed for offshore wind conditions) was selected. The technical specifications of the wind turbine can be found in https://en.wind-turbine-models.com/turbines/1419-mhi-vestas-offshore-v164-8.0-mw (last accessed 15 September 2021) and the corresponding power curve P_{WT} can be found in [54].

The mean power output of the Vestas V164-8.0 wind turbine at a specific location, where a discrete and sufficiently long time series of wind speeds u_i, $i = 1, 2, \cdots, n$, with a

1 h–time step (as is the time step of the ERA5 wind dataset in our case) is available, can be simply estimated as follows:

$$\overline{P}_W = \frac{1}{N} \sum_{i=1}^{N} P_{WT}(u_i)$$ (17)

where $P_{WT}(\cdot)$ is the corresponding power curve and N is the available sample size. The mean annual values of $P_{W,j}$, $j = 1, 2, \cdots, J$ for year j, can be estimated in a straightforward way, while the corresponding annual energy output for year j, $E_{W,j}$, $j = 1, 2, \cdots, J$ can be obtained by integrating $P_{W,j}$ over each year.

For $P_{WT}(\cdot)$ in kW, E_W is expressed in kWh. Although power curve modeling is frequently used in similar applications, see, e.g., [55], in this work, direct use is made of the wind turbine power curve as is provided in [54]. When it was required, linear interpolation was performed for estimating E_W at particular wind speeds.

The mean annual wind energy output $\overline{E}_{W,AN}$ can then be estimated as follows:

$$\overline{E}_{W,AN} = \frac{1}{J} \sum_{j=1}^{J} E_{W,j}$$ (18)

where J is the total of years (20 in our case).

For the exploitation of wave energy, the Pelamis wave energy converter was selected. The power characteristics $P_{VP}(H_S, T_e)$ of the Pelamis WEC are described in [56]. Following the same approach as above, the mean wave power output can be estimated as follows:

$$\overline{P}_V = \frac{1}{N} \sum_{i=1}^{N} P_{VP}(H_{S,i}, T_{e,i})$$ (19)

where N is the number of (H_S, T_e)–sea states, and $P_{VP}(H_{S,i}, T_{e,i})$ is the power matrix of the Pelamis WEC. The mean annual values of $P_{V,j}$, $j = 1, 2, \cdots, J$ for year j, can be estimated in a straightforward way, while the corresponding annual energy output for year j, $E_{V,j}$, $j = 1, 2, \cdots, J$ can be obtained by integrating $P_{V,j}$ over each year.

The mean annual wave energy output can then be estimated as follows:

$$\overline{E}_{V,AN} = \frac{1}{J} \sum_{j=1}^{J} E_{V,j}$$ (20)

where J is the total of years.

The energy output, using the above methods for the Vestas wind turbine and the Pelamis wave energy converter, respectively, was estimated for the two most favorable locations that are identified in the previous section, in terms of complementarity (A) and synergy (B). The results are summarized in Table 5, including a layout of 1×12 Pelamis WECs, in order to achieve a nominal power close to 8 MW, resulting in a farm of a total capacity of 9 MW (12×750 kW).

Table 5. Energy outputs of Vestas offshore wind turbine and Pelamis devices in best complementarity (A) and synergy (B) points.

Device	Point A [38° N, 26.5° E]	Point B [35° N, 27.5° E]
1 Vestas (GWh)	33.080	34.406
1 Pelamis (MWh)	64.280	347.321
1 × 12 Array of Pelamis (MWh)	771.360	4167.852

The efficiency of the attenuator's WECs is dependent on the mean wave direction, see [57] and references cited therein. On the other hand, phenomena like diffraction and

reflection usually occur inside the area of WEC array installation, as the presence of the wave farms affects the directional spreading and the wave spectral shape while it also reduces the amplitude of the sea waves. For quantification purposes, a coefficient called energy transmission factor, represents the percentage of energy remaining in the sea after the waves pass through the WEC array. Another factor called the "capture width" defines the length of the wave crest that is absorbed by the instrument and varies with both wave height and wave period. Transmission factors for WECs are partially commercially confidential, yet they have a dynamic behavior depending especially on the magnitude of the significant wave height and wave period [58]. The spatial distribution in wave power in the vicinity of a wave farm is strongly dependent on the device-incident wave climate and the device absorption parameters. In WEC locations, large reductions (~25%) in wave power leeward of the devices may occur [59]. Therefore, for an optimized operation, Pelamis arrays are better installed in a single line or in a two-row array. In this respect, as well as taking into account that the contribution of the aforementioned transmission factors is practical under specific basin modeling scenarios, an array of 1 × 12 Pelamis devices is examined (see Table 5), avoiding energy output reductions, due to the attenuated waves at the leeward section of the installation and the direction of the incident, diffracted and reflected ones inside the farm. Moreover, it can be easily seen that the WEC arrays located in point B (i.e., the location with the best synergy value), produce larger amounts of wave energy, while offshore wind energy is similar in both locations.

5. Conclusions

Joint offshore wind and wave energy exploitation seems to be one of the most promising solutions to compensate for the continuously increasing energy demand and high costs of offshore wind energy. The Greek Seas are characterized by a remarkable offshore wind power potential; thus, the main objective of this paper was to identify favorable locations for collocating hybrid offshore wind and wave energy systems. This was performed by assessing the wind and wave energy complementarity of the Greek Seas using ERA5 data. Firstly, the ERA5 reanalysis dataset was evaluated by means of in-situ measurements derived from six Poseidon buoys. It was concluded that there is a strong correlation between the datasets, and that the ERA5 tends to underestimate the actual values of the measured parameters.

In terms of energy potential, offshore wind has maximum wind power density values of the order of 650–800 W/m^2 that are encountered across the central axis of Aegean Sea, an area that is characterized by strong northern winter and summer winds (Etesian winds). In addition, wave energy flux peak values range between 5–7 kW/m in west, southwest and southeast areas of Crete Isl., an area characterized by large fetch lengths that allow the development of larger wind waves and swells. In this respect, the most favorable locations in terms of complementarity and synergy were, respectively, identified as follows: southeast of Chios Isl. (point A: 38° N, 26.5° E—index value 45.143%) and southeast of Karpathos Isl. (point B: 35° N, 27.5° E—index value 29.261%), taking into consideration a threshold value of 300 m water depth.

In the context of an actual application in the aforementioned locations, an 8-MW offshore wind turbine and an array of 1 × 12 Pelamis WECs (750 kW each) could produce at point A an annual energy output of 33.080 GWh and 771.360 MWh, respectively, while the same hybrid system at point B could generate 34.406 GWh of wind energy and 4167.852 MWh of wave energy in the same temporal scale. The difference between the annual energy output from the WEC between locations A and B can be explained by the fact that the grid point with the highest synergy index is located in an area characterized by large fetch lengths and thus higher wave energy potential.

Author Contributions: Conceptualization, T.S.; methodology, T.S.; software, K.K. and I.B.; validation, K.K. and I.B.; formal analysis, T.S., K.K. and I.B.; investigation, K.K. and I.B.; writing—original draft preparation, T.S., K.K. and I.B.; writing—review and editing, T.S., K.K. and I.B.; All authors have read and agreed to the published version of the manuscript.

References

1. Soukissian, T.H.; Denaxa, D.; Karathanasi, F.; Prospathopoulos, A.; Sarantakos, K.; Iona, A.; Georgantas, K.; Mavrakos, S. Marine Renewable Energy in the Mediterranean Sea: Status and Perspectives. *Energies* **2017**, *10*, 1512. [CrossRef]
2. Soukissian, T. Use of multi-parameter distributions for offshore wind speed modeling: The Johnson SB distribution. *Appl. Energy* **2013**, *111*, 982–1000. [CrossRef]
3. Johnston, B.; Foley, A.; Doran, W.J.; Littler, T. Levelised cost of energy, A challenge for offshore wind. *Renew. Energy* **2020**, *160*, 876–885. [CrossRef]
4. Rubio-Domingo, G.; Linares, P. The future investment costs of offshore wind: An estimation based on auction results. *Renew. Sustain. Energy Rev.* **2021**, *148*, 111324. [CrossRef]
5. Lavidas, G.; Blok, K. Shifting wave energy perceptions: The case for wave energy converter (WEC) feasibility at milder resources. *Renew. Energy* **2021**, *170*, 1143–1155. [CrossRef]
6. Besio, G.; Mentaschi, L.; Mazzino, A. Wave energy resource assessment in the Mediterranean Sea on the basis of a 35-year hindcast. *Energy* **2016**, *94*, 50–63. [CrossRef]
7. Jin, S.; Greaves, D. Wave energy in the UK: Status review and future perspectives. *Renew. Sustain. Energy Rev.* **2021**, *143*, 110932. [CrossRef]
8. Soukissian, T.; Karathanasi, F. Joint Modelling of Wave Energy Flux and Wave Direction. *Processes* **2021**, *9*, 460. [CrossRef]
9. Mazarakos, T.; Konispoliatis, D.; Katsaounis, G.; Polyzos, S.; Manolas, D.; Voutsinas, S.; Soukissian, T.; Mavrakos, S.A. Numerical and experimental studies of a multi-purpose floating TLP structure for combined wind and wave energy exploitation. *Mediterr. Mar. Sci.* **2019**, *20*, 745–763. [CrossRef]
10. Konispoliatis, D.; Katsaounis, G.; Manolas, D.; Soukissian, T.; Polyzos, S.; Mazarakos, T.; Voutsinas, S.; Mavrakos, S. REFOS: A Renewable Energy Multi-Purpose Floating Offshore System. *Energies* **2021**, *14*, 3126. [CrossRef]
11. Pérez-Collazo, C.; Greaves, D.; Iglesias, G. A review of combined wave and offshore wind energy. *Renew. Sustain. Energy Rev.* **2015**, *42*, 141–153. [CrossRef]
12. McTiernan, K.L.; Sharman, K.T. Review of Hybrid Offshore Wind and Wave Energy Systems. *J. Physics Conf. Ser.* **2020**, *1452*, 012016. [CrossRef]
13. Azzellino, A.; Lanfredi, C.; Riefolo, L.; De Santis, V.; Contestabile, P.; Vicinanza, D. Combined Exploitation of Offshore Wind and Wave Energy in the Italian Seas: A Spatial Planning Approach. *Front. Energy Res.* **2019**, *7*, 42. [CrossRef]
14. Veigas, M.; Iglesias, G. Wave and offshore wind potential for the island of Tenerife. *Energy Convers. Manag.* **2013**, *76*, 738–745. [CrossRef]
15. Dalton, G.; Bardócz, T.; Blanch, M.; Campbell, D.; Johnson, K.; Lawrence, G.; Lilas, T.; Friis-Madsen, E.; Neumann, F.; Nikitas, N.; et al. Feasibility of investment in Blue Growth multiple-use of space and multi-use platform projects; results of a novel assessment approach and case studies. *Renew. Sustain. Energy Rev.* **2019**, *107*, 338–359. [CrossRef]
16. Gideon, R.A.; Bou-Zeid, E. Collocating offshore wind and wave generators to reduce power output variability: A Multi-site analysis. *Renew. Energy* **2021**, *163*, 1548–1559. [CrossRef]
17. Tedeschi, E.; Robles, E.; Santos, M.; Duperray, O.; Salcedo, F. Effect of energy storage on a combined wind and wave energy farm. In Proceedings of the 2012 IEEE Energy Conversion Congress and Exposition (ECCE), Raleigh, NC, USA, 15–20 September 2012; pp. 2798–2804.
18. Astariz, S.; Iglesias, G. Selecting optimum locations for co-located wave and wind energy farms. Part I: The Co-Location Feasibility index. *Energy Convers. Manag.* **2016**, *122*, 589–598. [CrossRef]
19. Rusu, L.; Ganea, D.; Mereuta, E. A joint evaluation of wave and wind energy resources in the Black Sea based on 20-year hindcast information. *Energy Explor. Exploit.* **2017**, *36*, 335–351. [CrossRef]
20. Fusco, F.; Nolan, G.; Ringwood, J. Variability reduction through optimal combination of wind/wave resources—An Irish case study. *Energy* **2010**, *35*, 314–325. [CrossRef]
21. Kalogeri, C.; Galanis, G.; Spyrou, C.; Diamantis, D.; Baladima, F.; Koukoula, M.; Kallos, G. Assessing the European offshore wind and wave energy resource for combined exploitation. *Renew. Energy* **2017**, *101*, 244–264. [CrossRef]

22. Astariz, S.; Iglesias, G. Enhancing Wave Energy Competitiveness through Co-Located Wind and Wave Energy Farms. A Review on the Shadow Effect. *Energies* **2015**, *8*, 7344–7366. [CrossRef]

23. Astariz, S.; Iglesias, G. Selecting optimum locations for co-located wave and wind energy farms. Part II: A case study. *Energy Convers. Manag.* **2016**, *122*, 599–608. [CrossRef]

24. Soukissian, T.H.; Karathanasi, F.E.; Zaragkas, D.K. Exploiting offshore wind and solar resources in the Mediterranean using ERA5 reanalysis data. *Energy Convers. Manag.* **2021**, *237*, 114092. [CrossRef]

25. Ferrari, F.; Besio, G.; Cassola, F.; Mazzino, A. Optimized wind and wave energy resource assessment and offshore exploitability in the Mediterranean Sea. *Energy* **2020**, *190*, 116447. [CrossRef]

26. Benassai, G.; Mariani, P.; Stenberg, C.; Christoffersen, M. A Sustainability Index of potential co-location of offshore wind farms and open water aquaculture. *Ocean Coast. Manag.* **2014**, *95*, 213–218. [CrossRef]

27. Weiss, C.V.; Ondiviela, B.; Guinda, X.; Del Jésus, F.; González, J.; Guanche, R.; Juanes, J.A. Co-location opportunities for renewable energies and aquaculture facilities in the Canary Archipelago. *Ocean Coast. Manag.* **2018**, *166*, 62–71. [CrossRef]

28. Monforti, F.; Huld, T.; Bódis, K.; Vitali, L.; D'Isidoro, M.; Arántegui, R.L. Assessing complementarity of wind and solar resources for energy production in Italy. A Monte Carlo approach. *Renew. Energy* **2014**, *63*, 576–586. [CrossRef]

29. Miglietta, M.M.; Huld, T.; Monforti-Ferrario, F. Local Complementarity of Wind and Solar Energy Resources over Europe: An Assessment Study from a Meteorological Perspective. *J. Appl. Meteorol. Clim.* **2017**, *56*, 217–234. [CrossRef]

30. Vega-Sanchez, M.A.; Castaneda-Jimenez, P.D.; Pena-Gallardo, R.; Ruiz-Alonso, A.; Morales-Saldana, J.A.; Palacios-Hernandez, E.R. Evaluation of complementarity of wind and solar energy resources over Mexico using an image processing approach. In Proceedings of the 2017 IEEE International Autumn Meeting on Power, Electronics and Computing (ROPEC), Ixtapa, Mexico, 8–10 November 2017; pp. 1–5. [CrossRef]

31. Prasad, A.; Taylor, R.A.; Kay, M. Assessment of solar and wind resource synergy in Australia. *Appl. Energy* **2017**, *190*, 354–367. [CrossRef]

32. Schindler, D.; Behr, H.D.; Jung, C. On the spatiotemporal variability and potential of complementarity of wind and solar resources. *Energy Convers. Manag.* **2020**, *218*, 113016. [CrossRef]

33. Ren, G.; Wan, J.; Liu, J.; Yu, D. Spatial and temporal assessments of complementarity for renewable energy resources in China. *Energy* **2019**, *177*, 262–275. [CrossRef]

34. Jurasz, J.; Canales, F.; Kies, A.; Guezgouz, M.; Beluco, A. A review on the complementarity of renewable energy sources: Concept, metrics, application and future research directions. *Sol. Energy* **2019**, *195*, 703–724. [CrossRef]

35. Ganea, D.; Amortila, V.; Mereuta, E.; Rusu, E. A Joint Evaluation of the Wind and Wave Energy Resources Close to the Greek Islands. *Sustainability* **2017**, *9*, 1025. [CrossRef]

36. Moschos, E.; Manou, G.; Dimitriadis, P.; Afentoulis, V.; Koutsoyiannis, D.; Tsoukala, V.K. Harnessing wind and wave resources for a Hybrid Renewable Energy System in remote islands: A combined stochastic and deterministic approach. *Energy Procedia* **2017**, *125*, 415–424. [CrossRef]

37. Loukogeorgaki, E.; Vagiona, D.G.; Vasileiou, M. Site Selection of Hybrid Offshore Wind and Wave Energy Systems in Greece Incorporating Environmental Impact Assessment. *Energies* **2020**, *11*, 2095. [CrossRef]

38. Hersbach, H.; Bell, B.; Berrisford, P.; Hirahara, S.; Horanyi, A.; Muñoz-Sabater, J.; Nicolas, J.; Peubey, C.; Radu, R.; Schepers, D.; et al. The ERA5 global reanalysis. *Q. J. R. Meteorol. Soc.* **2020**, *146*, 1999–2049. [CrossRef]

39. Hersbach, H.; Bell, B.; Berrisford, P.; Biavati, G.; Horányi, A.; Muñoz Sabater, J.; Nicolas, J.; Peubey, C.; Radu, R.; Rozum, I.; et al. *ERA5 Hourly Data on Single Levels From 1979 to Present*; Copernicus Climate Change Service (C3S) Climate Data Store (CDS). Available online: https://cds.climate.copernicus.eu/cdsapp#!/dataset/reanalysis-era5-single-levels?tab=overview (accessed on 3 March 2021). [CrossRef]

40. Farjami, H.; Hesari, A.R.E. Assessment of sea surface wind field pattern over the Caspian Sea using EOF analysis. *Reg. Stud. Mar. Sci.* **2020**, *35*, 101254. [CrossRef]

41. Tavares, L.F.D.A.; Shadman, M.; Assad, L.P.D.F.; Silva, C.; Landau, L.; Estefen, S. Assessment of the offshore wind technical potential for the Brazilian Southeast and South regions. *Energy* **2020**, *196*, 117097. [CrossRef]

42. Bruno, M.F.; Molfetta, M.G.; Totaro, V.; Mossa, M. Performance Assessment of ERA5 Wave Data in a Swell Dominated Region. *J. Mar. Sci. Eng.* **2020**, *8*, 214. [CrossRef]

43. Soukissian, T.; Chronis, G. Poseidon: A marine environmental monitoring, forecasting and information system for the Greek seas. *Mediterr. Mar. Sci.* **2000**, *1*, 71. [CrossRef]

44. Soukissian, T.H.; Chronis, G.T.; Nittis, K.; Diamanti, C. Advancement of Operational Oceanography in Greece: The Case of the Poseidon System. *J. Atmos. Ocean Sci.* **2002**, *8*, 93–107. [CrossRef]

45. Gower, J.F.R. Intercalibration of wave and wind data from TOPEX/POSEIDON and moored buoys off the west coast of Canada. *J. Geophys. Res. Space Phys.* **1996**, *101*, 3817–3829. [CrossRef]

46. Soukissian, T.; Kechris, C. About applying linear structural method on ocean data: Adjustment of satellite wave data. *Ocean Eng.* **2007**, *34*, 371–389. [CrossRef]

47. Soukissian, T.H.; Karathanasi, F.E.; Voukouvalas, E.G. Effect of outliers in wind speed assessment. In Proceedings of the Proceedings of the 24th International Ocean and Polar Engineering Conference, Busan, Korea, 15–20 June 2014; pp. 362–369.

48. Karathanasi, F.E.; Soukissian, T.H.; Axaopoulos, P.G. Calibration of wind directions in the Mediterranean Sea. In Proceedings of the International Ocean and Polar Engineering Conference, Rhodes, Greece, 26 June–1 July 2016; pp. 491–497.

49. Soukissian, T.; Papadopoulos, A. Effects of different wind data sources in offshore wind power assessment. *Renew. Energy* **2015**, *77*, 101–114. [CrossRef]

50. Guillou, N. Estimating wave energy flux from significant wave height and peak period. *Renew. Energy* **2020**, *155*, 1383–1393. [CrossRef]

51. Soukissian, T.; Papadopoulos, A.; Skrimizeas, P.; Karathanasi, F.; Axaopoulos, P.; Avgoustoglou, E.; Kyriakidou, H.; Tsalis, C.; Voudouri, A.; Gofa, F.; et al. Assessment of offshore wind power potential in the Aegean and Ionian Seas based on high-resolution hindcast model results. *AIMS Energy* **2017**, *5*, 268–289. [CrossRef]

52. Soukissian, T.H.; Gizari, N.; Chatzinaki, M. Wave potential of the Greek seas. In Proceedings of the WIT Transactions on Ecology and the Environment, Alicante, Spain, 11–13 April 2011; pp. 203–213.

53. Lin, Z.; Liu, X.; Lotfian, S. Impacts of water depth increase on offshore floating wind turbine dynamics. *Ocean Eng.* **2021**, *224*, 108697. [CrossRef]

54. Pandit, R.; Kolios, A. SCADA Data-Based Support Vector Machine Wind Turbine Power Curve Uncertainty Estimation and Its Comparative Studies. *Appl. Sci.* **2020**, *10*, 8685. [CrossRef]

55. Sohoni, V.; Gupta, S.C.; Nema, R.K. A Critical Review on Wind Turbine Power Curve Modelling Techniques and Their Applications in Wind Based Energy Systems. *J. Energy* **2016**, *2016*, 8519785. [CrossRef]

56. Marañon-Ledesma, H.; Tedeschi, E. Energy storage sizing by stochastic optimization for a combined wind-wave-diesel supplied system. In Proceedings of the 2015 International Conference on Renewable Energy Research and Applications (ICRERA), Palermo, Italy, 22–25 November 2015; pp. 426–431.

57. Soukissian, T. Probabilistic modeling of directional and linear characteristics of wind and sea states. *Ocean Eng.* **2014**, *91*, 91–110. [CrossRef]

58. Rusu, E.; Soares, C.G. Coastal impact induced by a Pelamis wave farm operating in the Portuguese nearshore. *Renew. Energy* **2013**, *58*, 34–49. [CrossRef]

59. Greenwood, C. The Impact of Large Scale Wave Energy Converter Farms on the Regional Wave Climate. Ph.D. Thesis, University of the Highlands and Islands and The University of Aberdeen, Aberdeen, UK, 2015.